Angewandte
International Edition *Chemie*

Self-Assembly

Self-Organization of Hydrogen-Bonding Naphthalene Chromophores into J-type Nanorings and H-type Nanorods: Impact of Regioisomerism**

Shiki Yagai,* Yusaku Goto, Xu Lin, Takashi Karatsu, Akihide Kitamura, Daiki Kuzuhara, Hiroko Yamada, Yoshihiro Kikkawa, Akinori Saeki, and Shu Seki

Nature has evolved complex self-organized architectures of pigment assemblages with rational nanoscale topologies and chromophore orientation.[1] Circular architectures of the chlorophyll–protein complexes found in the light-harvesting systems of purple photosynthetic bacteria could be regarded as perfect supramolecular assemblies of pigments in view of not only their topological features but also a functional standpoint.[1b,2] Sunlight is absorbed uniformly by circularly organized chlorophyll pigments, and the resulting exciton states are delocalized over the closed arrays of chlorophylls.[3] Such exciton delocalization is achieved by partially overlapped arrays of chlorophyll π systems, which could be referred to as J-type (offset) stacking.[4] In contrast, one-dimensional stacks of largely overlapped π systems, which can be referred to as H-type (face-to-face) stacking, are promising as quasi one-dimensional pathways of mobile charge carriers for organic electronics.[5] Thus, these natural and artificial assemblies of π systems show the importance of simultaneous control over dimensionality of nanostructures and local stacking arrangements to optimize the functionality in the

systems. Herein we report that a regioisomerism in specifically designed self-assembling small molecules can offer the aforementioned two extreme nanoarchitectures with favorable stacking arrangements of their π systems.

We have recently reported the self-assembly of π-conjugated molecules substituted asymmetrically with barbituric acid (BAR) and a wedge-shaped aliphatic tail ("minidendron"[6]).[7] An unique feature of these BAR–π-wedge molecules in nonpolar media is that their ability to form dramatically different nanostructures, namely nanorings[7a,b,8] and nanorods,[7c] depending on the structure of the π moiety. X-ray diffraction analysis in the mesomorphic state suggested that the BAR–π-wedge molecules form columnar stacks of hydrogen-bonded hexamers (rosettes), which are in nonpolar media solvated to form curved (for nanorings) or straight nanostructures (for nanorods). Although this molecular design is attractive for the construction of well-defined nanostructures consisting of functional π systems, it remains difficult to clarify the structural relationship between monomers and assemblies. We now report a striking impact of the regioisomerism of BAR–naphthalene-wedge molecules (Figure 1) on their self-assembled nanostructures, which

[*] Prof. Dr. S. Yagai, Y. Goto, Dr. X. Lin, Prof. Dr. T. Karatsu,
Prof. Dr. A. Kitamura
Department of Applied Chemistry and Biotechnology
Graduate School of Engineering, Chiba University
1-33 Yayoi-cho, Inage-ku, Chiba 263-8522 (Japan)
E-mail: yagai@faculty.chiba-u.jp

Dr. D. Kuzuhara, Prof. Dr. H. Yamada
Graduate School of Material Science
Nara Institute of Science and Technology (NAIST)
8916-5, Takayama-cho, Ikoma, Nara 630-0192 (Japan)

Prof. Dr. S. Yagai, Prof. Dr. H. Yamada
CREST, JST, 5-3, Yonbancho, Chiyoda-ku
Tokyo 102-8666 (Japan)

Dr. Y. Kikkawa
National Institute of Advanced Industrial Science and Technology
(AIST)
1-1-1 Higashi, Tsukuba, Ibaraki 305-8562 (Japan)

Dr. A. Saeki, Prof. Dr. S. Seki
Department of Applied Chemistry
Graduate School of Engineering, Osaka University
2-1, Yamadaoka, Suita, Osaka 565-0871 (Japan)

Supporting information for this article is available on the WWW
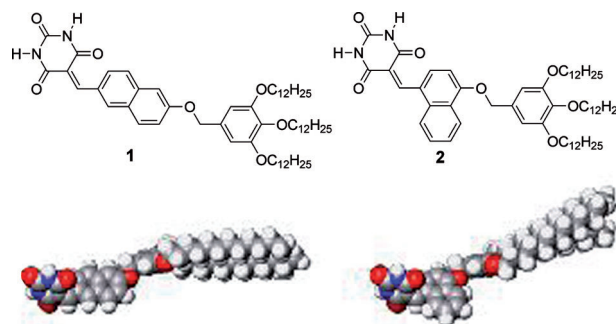under http://dx.doi.org/10.1002/anie.201201436.

Figure 1. Structures of BAR–naphthalene-wedge molecules **1** and **2** and their geometry-optimized structures.

imparts an important guide to this molecular design toward tailor-made nanostructures. Introduction of BAR and wedge functional moieties into different positions on the naphthalene core affords the rosettes with different geometrical features that are favorable for offset or face-to-face stacking arrangements. This geometrical difference at the level of rosettes not only yields perfect nanorings and nanorods, but also enables favorable J- and H-type excitonic coupling of the naphthalene cores, thus exhibiting distinct optical features.

© 2012 Wiley-VCH Verlag GmbH & Co. KGaA, Weinheim

Regioisomers **1** (substituted at the 2,6-positions) and **2** (1,4-positions) were prepared according to the reported method[7a] and fully characterized by NMR, MS, and elemental analysis.[9] The naphthalene rings in these regioisomers are rotatable in the axis connecting their substituted positions. Regioisomer **2**, the naphthalene ring of which is substituted on its short molecular axis, may have a greater steric repulsion with neighboring molecules compared to **1** when they assemble into rosette architectures. This may lead to a greater rotational twisting of the naphthalene rings in rosette **2**$_6$ compared to rosette **1**$_6$, thus imparting these rosettes with different morphological features.

The UV/Vis absorption spectra of methylcyclohexane (MCH) solutions of **1** and **2** recorded at 70°C exhibited vibronic transitions characteristic of molecularly dissolved π systems (red lines in Figure 2a,b). Upon cooling, the
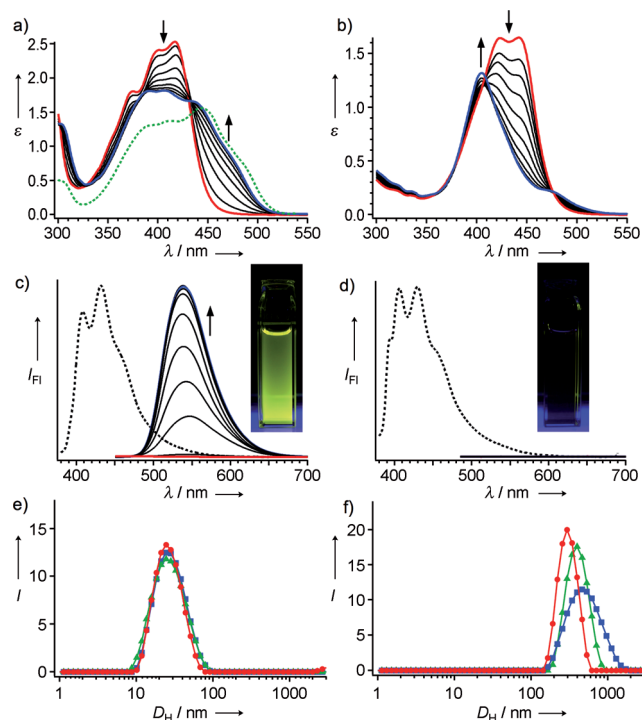

Figure 2. Temperature-dependent a,b) UV/vis spectra and c,d) fluorescence spectra of a,c) **1** and b,d) **2** at a concentration of 1×10^{-4} M. Left axes in (a,b) are shown with molar extinction coefficient ε in 10^4 L mol^{-1} cm^{-1}. The spectra were recorded upon cooling from 70°C (red) to 20°C (blue) at 10°C intervals. The arrows indicate changes upon cooling. Insets in (c,d) are photographs of the solutions at 20°C under UV light illumination. The green dotted spectrum in (a) is a fluorescence excitation spectrum of **1** monitored at 550 nm. e,f) Dynamic light scattering of e) **1** and f) **2** in MCH at concentrations of 5×10^{-5} M (red), 1×10^{-4} M (green), and 5×10^{-4} M (blue).

formation of different types of aggregates was revealed for these regioisomers by distinct spectral changes. Regioisomer **1** displayed a pronounced growth of bathochromically shifted absorption bands (blue line in Figure 2a). The spectrum recorded at 20°C showed an increase of the integrated molar absorptivity in the range of 300–550 nm ($\varepsilon_{i(300-550)}$) from 380 L mol^{-1} cm^{-1} at 70°C to 442 L mol^{-1} cm^{-1}. Such spectral

changes are clear indications of the J-type stacking of the aromatic chromophores.[10] In striking contrast, regioisomer **2** showed a hypsochromic shift ($\lambda_{max} = 442 \rightarrow 405$ nm) together with a significant hypochromic effect upon cooling (blue line in Figure 2b). The presence of red-shifted absorption shoulder at 470 nm indicates a twisted stacking arrangement of naphthalene chromophores.[11] The $\varepsilon_{i(300-550)}$ value of **2** decreased from 251 to 176 L mol^{-1} cm^{-1} upon going from 70 to 20°C. These spectral changes are typical of the formation of H-type stacking of aromatic molecules.

According to exciton theory,[12] J-type aggregation of dyes open radiative decay pathway for the excited states, whereas H-type aggregation results in nonradiative decay. Regioisomers **1** and **2**, when they are monomeric in tetrahydrofuran, weakly fluoresce with structured emission bands (dotted lines in Figure 2c,d). The low fluorescence quantum yields ($\Phi_{FL} \approx 0.0003$) are attributed to nonradiative deactivation by a bond-twisting in the excited states. On the other hand, monomeric species in MCH at 70°C became almost non-emissive owing to enhanced thermal deactivation (red lines in Figure 2c,d). With decreasing temperature, however, a prominent emission was observed for **1** at 550 nm (Figure 2c). The fluorescence quantum yield measured for the 1×10^{-4} solution increased to 0.08 at 20°C. This was not the case for **2**, which remained non-emissive upon decreasing the temperature (Figure 2d). Although the enhanced emission of **1** is partly due to the suppression of bond-twisting by aggregation,[13] contrastive emission properties of these regioisomers in the aggregated state further exemplify the distinct stacking arrangements of naphthalene chromophores.

Dynamic light scattering (DLS) measurements were performed for MCH solutions of **1** and **2** at three concentrations: 5×10^{-5}, 1×10^{-4}, and 5×10^{-4} M. For **1**, average hydrodynamic diameters (D_H) of ca. 29 nm were always observed upon changing the concentration (Figure 2e). The concentration-independent D_H is a clear indication of the formation of stable closed aggregates. On the contrary, regioisomeric **2** displayed D_H of 310 nm already at 5×10^{-5} M (Figure 2f), which is one order of magnitude larger than that of **1**. More importantly, **2** showed a concentration-induced increase of D_H to 410 nm at 1×10^{-4} M and to 540 nm at 5×10^{-4} M. This observation suggests the formation of open-ended aggregates.

We used atomic force microscopy (AFM) to unveil the dramatically different nanostructures of the aggregates. Figure 3a is the AFM image of J-aggregated **1** spin-coated from a MCH solution onto highly oriented pyrolytic graphite (HOPG). Perfectly toroidal nanostructures (nanorings) were observed (Supporting Information, Figure S1). These nanorings have remarkable uniformity in their height and size: the height (h_{ring}) is (2.0 ± 0.1) nm, and the top-to-top diameter ($d1_{ring}$) is (14 ± 0.1) nm (Figure 3c). The edge-to-edge diameter ($d2_{ring}$) after accounting for the tip broadening effect is (20 ± 0.1) nm. Any other nanostructures could be scarcely found by repeated AFM imaging in different areas. Remarkably, nanorings could be exclusively imaged for samples prepared from solutions with a wide concentration range between 5×10^{-5} M and 5×10^{-3} M. This situation is notably different from our previous BAR–π-wedge assemblies, for
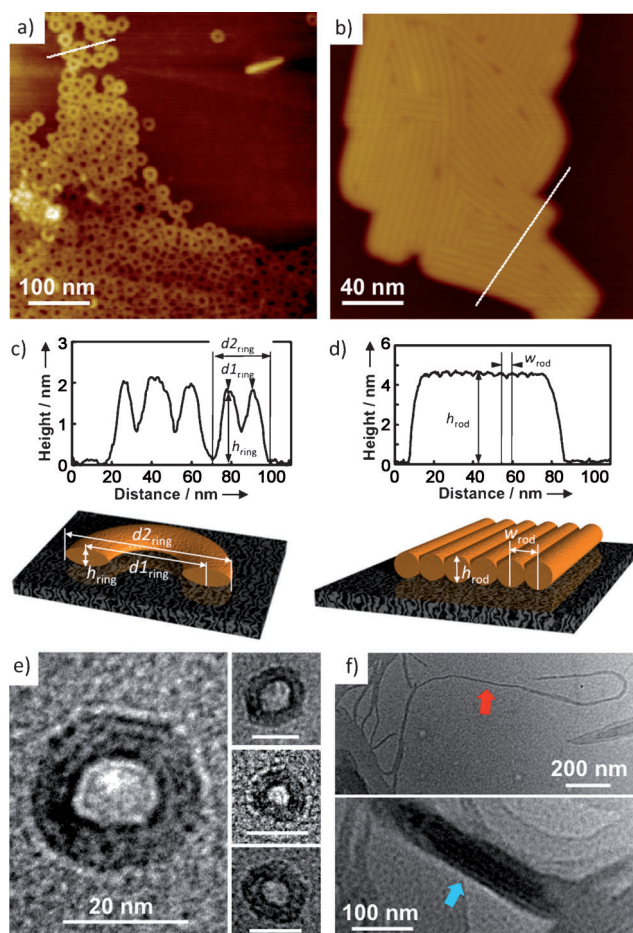
Figure 3. a,b) AFM height images of a) **1** and b) **2** spin-coated from MCH solutions (**1**: $c = 5 \times 10^{-4}$ M; **2**: $c = 1 \times 10^{-4}$ M) onto HOPG. c,d) Cross-sectional analysis along the white lines in (a) and (b), respectively, with a representation of the nanostructures. e,f) TEM images of e) **1** (scale bars = 20 nm) and b) **2**. The red and blue arrows in (f) denote the isolated and bundled nanorods, respectively.

which increasing concentration resulted in the formation of open-ended nanofibers.[7a,c]

In strong contrast, AFM images of the H-aggregates of **2** displayed monolayers of densely packed rodlike nanostructures (nanorods). The monolayers consist of domains of 3–10 oriented nanorods (Figure 3b; Supporting Information, Figure S2). The heights of nanorods (h_{rod}) are uniform at (4.6 ± 0.1) nm, and the average top-to-top distance (w_{rod}) between neighboring rods is 5.6 nm (Figure 3d). Taking into account the deformation of nanorods by the adsorption to the substrate and the local tip force, the similarity in these dimensions suggests that the formation of cylindrical nanorods with the circular cross-section. For samples prepared from more dilute solutions (ca. 5×10^{-5} M), isolated nanorods could be imaged (Supporting Information, Figure S3), whose edge-to-edge width reaches 19.2 nm. For such isolated nanostructures, the tip-broadening effect is pronounced and calculated to be 13.3 nm according to the reported method.[14] The actual diameter of the isolated nanorods thus can be estimated as 5.9 nm, which is in good agreement

with the top-to-top distance estimated for the densely packed nanorods.

The foregoing nanostructures were further corroborated by transmission electron microscopy (TEM). For nanorings of **1** (Figure 3e), their edge-to-edge diameters ($d2_{ring}$) in the TEM images diverged in the range between 18 and 27 nm, which might be due to the deformation by vacuum evaporation. For **2**, both isolated and bundled nanorods could be seen (Figure 3f). Thus, the two regioisomers undergo specific organization process in solution where J-type and H-type π–π stacking of their naphthalene cores plays a key role to determine the nanostructures.

To obtain insight into the mechanism underlying the contrastive organization process and optical properties of the regioisomers in solution, their organization in the bulk state was investigated. Differential scanning calorimetry (DSC) and polarized optical microscopy (POM) revealed that both the compounds form thermotropic liquid crystalline mesophases in different temperature ranges (Figure 4 a,b).[15]
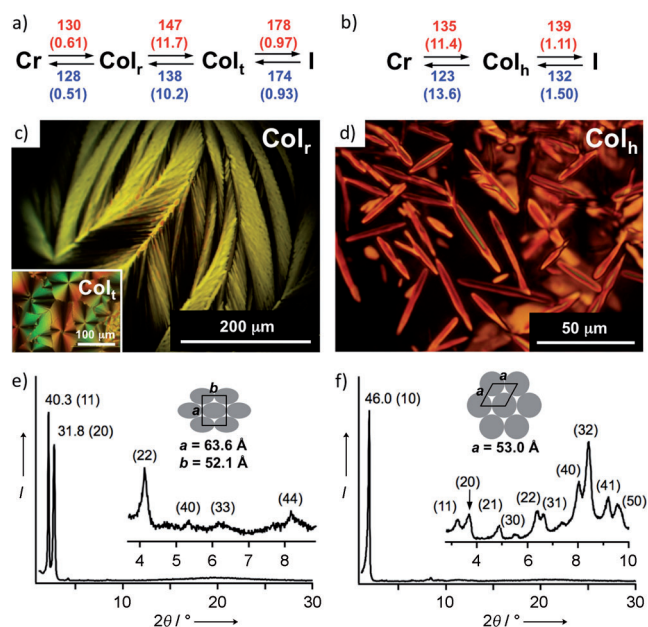

Figure 4. a,b) Thermal phase-transition behavior of a) **1** and b) **2** studied by DSC; transition temperatures are shown, with enthalpies in parentheses. c,d) Polarized optical micrographs and e,f) X-ray diffraction patterns of c,e) **1** in the Col$_r$ phase and d,f) **2** in the Col$_h$ phase. For **1**, POM texture of the Col$_t$ phase observed at a higher temperature is shown as an inset in image (c).

Regioisomer **1** showed two mesomorphic states with the boundary at 147 °C. POM observation upon cooling from the isotropic phase first exhibited a fan-shape texture typical of columnar liquid crystals, which upon further cooling turned to be a palmleaf-like texture at around 147 °C (Figure 4c). The X-ray diffraction (XRD) pattern of the higher-temperature mesophase showed the formation of tetragonal columnar structure (Col$_t$) with the lattice constant $a = 40.7$ Å (Supporting Information, Figure S4). On the other hand, the lower-temperature mesophase exhibited two explicit diffractions at $d = 40.3$ and 31.8 Å, diagnostic of a rectangular columnar

(Col$_r$) ordering (Figure 4e). The presence of minor higher-order diffractions allows the assignment of this phase as a *c2mm* centered rectangular columnar (Col$_r$) structure with lattice constant $a = 63.6$ and $b = 52.1$ Å.

Regioisomer **2** formed a mesophase in a very narrow temperature range (Figure 4b), and exhibited high-aspect-ratio linear defects upon cooling from the isotropic liquid (Figure 4d). XRD measurement of this mesophase displayed an intense diffraction peak at $d = 46.0$ Å with a lot of minor peaks that were perfectly assignable to diffractions from a hexagonal columnar structure with the lattice constant $a = 53.0$ Å (Figure 3f). The lattice constant is in good agreement with the width of nanorods estimated by AFM. The absence of focal-conic defect may reflect the formation of an exceptionally stiff columnar assemblies in the bulk state.[16]

By using synchrotron radiation, we could observed the intracolumnar periodicity of 3.6 Å (lattice constant *c* or center-to-center distance of stacked disks) for the Col$_h$ mesophase of **2** (Supporting Information, Figure S5). This periodicity allows the calculation of the number of molecules in a columnar slice of 3.6 Å thickness (*Z* value).[17] Assuming the density of **2** to be 1.0 g cm^{-3} from structurally related compounds,[18] the *Z* value is calculated to be 6.0, which strongly supports our previous hypothesis that BAR–π-wedge molecules form hexameric hydrogen-bonded rosettes.[7] On the other hand, the Col$_r$ mesophase of **1** showed no diffractions that could be assigned to the intracolumnar periodicity. We thus calculated its lattice constant *c* by giving $Z = 6$ for a columnar slice of *c* Å thickness. The calculated lattice constant *c* is 5.3 Å, which is notably longer than that of the Col$_h$ phase of **2**. The longer intracolumnar periodicity is typical of rectangular columnar organization of discotics, which is generally caused by a translational displacement to form columns with ellipsoidal cross-section.[17, 19]

The above XRD study clearly shows that the stacking arrangements of the rosettes play a crucial role in their hierarchical organization process. Molecular models of rosettes **1**$_6$ and **2**$_6$ are shown in Figure 5a. The two rosettes displayed a clear geometrical difference arising from the conformation of naphthalene moieties. Rosette **1**$_6$ shows a relatively flat geometry because six naphthalene rings do not rotate significantly owing to the absence of steric repulsion with neighboring molecules. For such a planar discotic entity with coplanar naphthalene moieties with respect to the rosette plane, a lateral displacement would occur upon stacking to minimize repulsive interaction between π surface,[20] which is consistent with the Col$_r$ packing in the mesophase. In aliphatic solvents, such a columnar stack of rosettes covered by aliphatic wedges is well-solvated and isolated, and lateral and most likely rotational displacement between rosettes engender a spontaneous curvature of columns, thus leading to the formation of nanorings (Figure 5b). It can be easily seen from simple geometrical considerations that neither translational nor rotational displacement of the rosette could give rise to an identical J-type stacking arrangement for all the six naphthalene moieties within a rosette. This situation is consistent with a rather broad absorption band of fully aggregated **1** in MCH (Figure 2a); the remaining absorption around 400 nm indicates
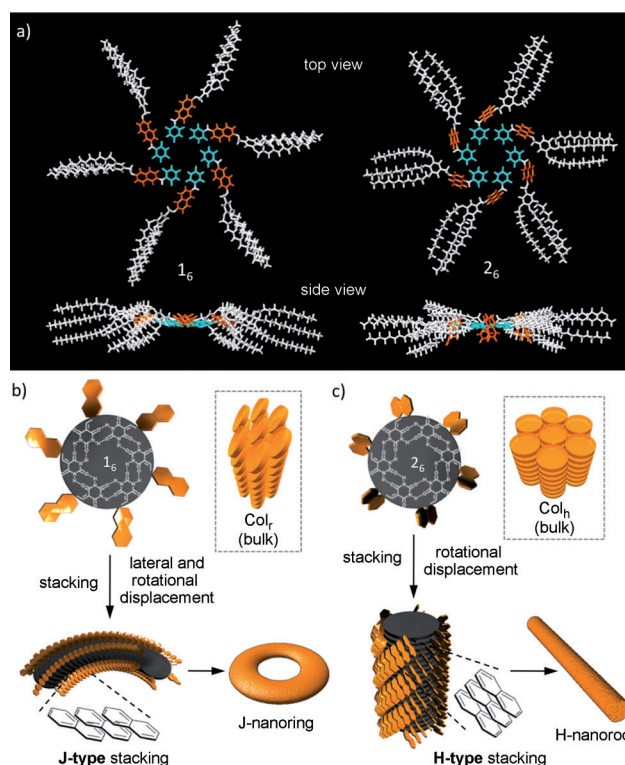

Figure 5. a) Geometry-optimized (MMFF) structures of hexameric rosettes of molecular modeled hexameric rosettes of **1** and **2**. b,c) Representation of the hierarchical organization of rosettes b) **1**$_6$ and c) **2**$_6$.

the existence of excitonically decoupled naphthalene chromophores. The fluorescence excitation spectrum of fully aggregated **1** monitored at 550 nm indeed showed a low contribution of these higher-energy bands to the green emission (green dotted curve in Figure 2a).

In contrast, rosette **2**$_6$ shows a crown-gear-like morphology owing to the rotation of six naphthalene rings to cancel the steric repulsion with neighboring molecules. For the stacking of such discotics, lateral displacement should not be allowed owing to steric hindrance induced by out-of-plane naphthalene moieties. Instead, a rotational displacement of the rosette would allow an optimal stacking arrangement[21] whereby out-of-plane naphthalene moieties can take a H-type π–π stacking interactions with a local rotational displacement, as seen by the red-shifted absorption shoulder (Figure 2b). The extension of this stacking model leads to the formation of a cylindrical rod featuring helical H-aggregates of naphthalene chromophores (Figure 5c).[22]

To obtain insight into the optoelectronic properties of the above nanostructures, we performed flash-photolysis time-resolved microwave conductivity (FP-TRMC) experiments, which enable electrodeless evaluation of photogenerated mobile charge carriers over a short distance (about 10 nm).[23] Upon excitation with a 355 nm laser pulse, the nanorings of **1** showed the maximum transient conductivity $\phi\Sigma\mu_{max}$ of 1.1×10^{-5} cm^2 V^{-1} s^{-1} (where ϕ = quantum yield of photocarrier generation and $\Sigma\mu$ = sum of the mobilities of photogenerated charge carriers; Figure S6). Remarkably, the nanorods of **2**

exhibited a value $\phi\Sigma\mu_{max}$ of 4.7×10^{-5} cm^2 V^{-1} s^{-1}, which is more than four times higher than that of the nanorings. The significant difference observed between the transient conductivities of the two contrasting nanoscopic aggregates illustrates that the nanorods can act as a superior semiconducting nanomaterial compared to the nanorings owing to the larger overlap (H-type stacking) as well as uniform π–π stacking arrangements of the naphthalene π systems.[24]

In conclusion, we have demonstrated that the regioisomeric introduction of barbituric acid and an aliphatic wedge into the naphthalene π system enables perfect control over the self-assembled nanostructures of our BAR–π-wedge molecules. The formation of distinct 0D and 1D nanostructures (nanorings and nanorods) by the regioisomers is ascribable to offset and face-to-face stacking arrangements of hydrogen-bonded cyclic assemblies (rosettes). This is, in turn, attributed to the conformational difference of naphthalene moieties with respect to the plane of rosettes. Of particular interest is that such different stacking modes of the rosettes also induced the representative stacking arrangements of naphthalene chromophores, as revealed by their characteristic optical and optoelectronic properties. Such simultaneous control over stacking fashion and self-assembled nanostructures for functional π assemblies is one of the most challenging goals in this research field toward nanostructured materials with tailor-made dimensionality and functionality. The self-sorting study of the regioisomers and extension of the π systems in the BAR–π-wedge design are underway.

[1] a) T. Kondo, K. Yoshida, A. Nakagawa, T. Kawai, H. Tamura, T. Goto, *Nature* **1992**, *358*, 515–518; b) G. McDermott, S. M. Prince, A. A. Freer, A. M. Hawthornthwaite-Lawless, M. Z. Papiz, R. J. Cogdell, N. W. Isaacs, *Nature* **1995**, *374*, 517–521.

[2] X. Hu, A. Damjanovic, T. Ritz, K. Schulten, *Proc. Natl. Acad. Sci. USA* **1998**, *95*, 5935–5941.

[3] A. M. van Oijen, M. Ketelaars, J. Kohler, T. J. Aartsma, J. Schmidt, *Science* **1999**, *285*, 400–402.

[4] a) G. Scheibe, *Angew. Chem.* **1936**, *49*, 563; b) E. E. Jelley, *Nature* **1936**, *138*, 1009–1010; c) *J-Aggregates* (Ed.: T. Kobayashi), World Scientific, Singapore, **1996**.

[5] a) L. Schmidt-Mende, A. Fechtenkotter, K. Müllen, E. Moons, R. H. Friend, J. D. MacKenzie, *Science* **2001**, *293*, 1119–1122; b) A. M. van de Craats, J. M. Warman, K. Müllen, Y. Geerts, J. D. Brand, *Adv. Mater.* **1998**, *10*, 36–38; c) J. Wu, W. Pisula, K. Müllen, *Chem. Rev.* **2007**, *107*, 718–747; d) F. J. M. Hoeben, P. Jonkheijm, E. W. Meijer, A. P. H. J. Schenning, *Chem. Rev.* **2005**, *105*, 1491–1546; e) Z. Chen, A. Lohr, C. R. Saha-Moller, F. Würthner, *Chem. Soc. Rev.* **2009**, *38*, 564–584.

[6] a) B. M. Rosen, C. J. Wilson, D. A. Wilson, M. Peterca, M. R. Imam, V. Percec, *Chem. Rev.* **2009**, *109*, 6275–6540; b) T. Nakanishi, *Chem. Commun.* **2010**, *46*, 3425–3436.

[7] a) S. Yagai, S. Kubota, H. Saito, K. Unoike, T. Karatsu, A. Kitamura, A. Ajayaghosh, M. Kanesato, Y. Kikkawa, *J. Am. Chem. Soc.* **2009**, *131*, 5408–5410; b) S. Yagai, T. Kinoshita, Y. Kikkawa, T. Karatsu, A. Kitamura, Y. Honsho, S. Seki, *Chem. Eur. J.* **2009**, *15*, 9320–9324; c) S. Yagai, Y. Goto, T. Karatsu, A. Kitamura, Y. Kikkawa, *Chem. Eur. J.* **2011**, *17*, 13657–13660.

[8] For other self-assembled nanorings spontaneously formed in solution, see: a) J.-K. Kim, E. Lee, Z. Huang, M. Lee, *J. Am. Chem. Soc.* **2006**, *128*, 14022–14023; b) S. Yagai, S. Mahesh, Y. Kikkawa, K. Unoike, T. Karatsu, A. Kitamura, A. Ajayaghosh, *Angew. Chem.* **2008**, *120*, 4769–4772; *Angew. Chem. Int. Ed.* **2008**, *47*, 4691–4694; c) S. Yagai, H. Aonuma, Y. Kikkawa, S. Kubota, T. Karatsu, A. Kitamura, S. Mahesh, A. Ajayaghosh, *Chem. Eur. J.* **2010**, *16*, 8652–8661; d) H. Shao, J. Seifert, N. C. Romano, M. Gao, J. J. Helmus, C. P. Jaroniec, D. A. Modarelli, J. R. Parquette, *Angew. Chem.* **2010**, *122*, 7854–7857; *Angew. Chem. Int. Ed.* **2010**, *49*, 7688–7691.

[9] see the Supporting Information.

[10] a) F. Würthner, T. E. Kaiser, C. R. Saha-Möller, *Angew. Chem.* **2011**, *123*, 3436–3473; *Angew. Chem. Int. Ed.* **2011**, *50*, 3376–3410; b) G. Borzsonyi, R. L. Beingessner, T. Yamazaki, J.-Y. Cho, A. J. Myles, M. Malac, R. Egerton, M. Kawasaki, K. Ishizuka, A. Kovalenko, H. Fenniri, *J. Am. Chem. Soc.* **2010**, *132*, 15136–15139.

[11] U. Rösch, S. Yao, R. Wortmann, F. Würthner, *Angew. Chem.* **2006**, *118*, 7184–7188; *Angew. Chem. Int. Ed.* **2006**, *45*, 7026–7030.

[12] M. Kasha, H. R. Rawls, M. A. El-Bayoumi, *Pure Appl. Chem.* **1965**, *11*, 371–392.

[13] Y. Hong, J. W. Y. Lam, B. Z. Tang, *Chem. Soc. Rev.* **2011**, *40*, 5361–5388.

[14] a) H. J. Butt, R. Guckenberger, J. P. Rabe, *Ultramicroscopy* **1992**, *46*, 375–393; b) P. Samorí, V. Francke, T. Mangel, K. Müllen, J. P. Rabe, *Opt. Mater.* **1998**, *9*, 390–393.

[15] T. Kato, N. Mizoshita, K. Kishimoto, *Angew. Chem.* **2006**, *118*, 44–74; *Angew. Chem. Int. Ed.* **2006**, *45*, 38–68.

[16] C. Destrade, P. Foucher, H. Gasparoux, T. Nguyen Huu, A. M. Levelut, J. Malthete, *Mol. Cryst. Liq. Cryst.* **1984**, *106*, 121–146.

[17] K. Hatsusaka, K. Ohta, I. Yamamoto, H. Shirai, *J. Mater. Chem.* **2001**, *11*, 423–433.

[18] G. Ungar, V. Percec, M. N. Holerca, G. Johansson, J. A. Heck, *Chem. Eur. J.* **2000**, *6*, 1258–1266.

[19] a) S. Jin, Y. Ma, S. C. Zimmerman, S. Z. D. Cheng, *Chem. Mater.* **2004**, *16*, 2975–2977; b) S. Yagai, T. Nakajima, K. Kishikawa, S. Kohmoto, T. Karatsu, A. Kitamura, *J. Am. Chem. Soc.* **2005**, *127*, 11134–11139.

[20] C. A. Hunter, J. K. M. Sanders, *J. Am. Chem. Soc.* **1990**, *112*, 5525–5534.

[21] M. Peterca, V. Percec, M. R. Imam, P. Leowanawat, K. Morimitsu, P. A. Heiney, *J. Am. Chem. Soc.* **2008**, *130*, 14840–14852.

[22] V. Percec, M. Glodde, T. K. Bera, Y. Miura, I. Shiyanovskaya, K. D. Singer, V. S. K. Balagurusamy, P. A. Heiney, I. Schnell, A. Rapp, H. W. Spiess, S. D. Hudson, H. Duan, *Nature* **2002**, *417*, 384–387.

[23] a) F. C. Grozema, L. D. A. Siebbeles, J. M. Warman, S. Seki, S. Tagawa, U. Scherf, *Adv. Mater.* **2002**, *14*, 228–231; b) A. Acharya, S. Seki, A. Saeki, Y. Koizumi, S. Tagawa, *Chem. Phys. Lett.* **2005**, *404*, 356–360; c) T. Amaya, S. Seki, T. Moriuchi, K. Nakamoto, T. Nakata, H. Sakane, A. Saeki, S. Tagawa, T. Hirao, *J. Am. Chem. Soc.* **2009**, *131*, 408–409.

[24] S. Yagai, Y. Nakano, S. Seki, A. Asano, T. Okubo, T. Isoshima, T. Karatsu, A. Kitamura, Y. Kikkawa, *Angew. Chem.* **2010**, *122*, 10186–10190; *Angew. Chem. Int. Ed.* **2010**, *49*, 9990–9994.